

Near-Field Wideband Beamforming for Extremely Large Antenna Array

Mingyao Cui, Linglong Dai, Robert Schober, and Lajos Hanzo

Abstract

Extremely large antenna array for wideband communications is a promising technology to achieve Tbps data rate for the next-generation communications. However, due to the extremely large bandwidth and antenna array aperture, the near-field beam split effect will severely decrease the actual transmission rates, which has not been investigated in existing works. To solve this challenging problem, we first reveal the near-field beam split effect and analyze the corresponding array gain loss. Then, a piecewise-far-field model with piecewise-linear phase property is proposed to approximate the near-field channel, based on which we propose a phase-delay focusing method to effectively mitigate the near-field beam split effect. Moreover, a new metric called effective Rayleigh distance is defined, which is more accurate than the classical Rayleigh distance to distinguish the far-field and near-field regions for practical communications. Finally, theoretical and numerical results are provided to demonstrate the effectiveness of our methods.

Index Terms

Extremely large antenna array, wideband, near-field beam split, beamforming, Rayleigh distance.

M. Cui and L. Dai are with the Beijing National Research Center for Information Science and Technology (BNRist) as well as the Department of Electronic Engineering, Tsinghua University, Beijing 100084, China (e-mails: cmy20@mails.tsinghua.edu.cn, daill@tsinghua.edu.cn).

R. Schober is with the Institute for Digital Communications at Friedrich-Alexander University Erlangen-Nürnberg (FAU) (e-mail: robert.schober@fau.de).

L. Hanzo is with the Department of Electronics and Computer Science, University of Southampton, Southampton SO17 1BJ, U.K. (e-mail: lh@ecs.soton.ac.uk).

This work was funded in part by National Key R&D Program of China (No.2020YFB1805005) and in part by the National Natural Science Foundation of China (Grant No. 62031019).

I. INTRODUCTION

Large antenna array can improve the transmission rate by orders of magnitude, which has become a key technology in current communications [1]. In the future, extremely large antenna array [2], where the array aperture is dramatically increased, is promising to realize ultra-high speed transmission in various scenarios, e.g., 6G [3]–[5], Wi-Fi [6], and visible light communications [7]. In 6G communications, extremely large array can be utilized in distributed MIMO communications with *radio stripes* [3] and reconfigurable intelligent surface (RIS) aided communications [4], [5] to provide ultra-high gain beams to improve the spectrum efficiency. Then, for the next-generation Wi-Fi7 (IEEE 802.11be), it has been proposed to deploy extremely large arrays on the entire wall to enhance the coverage [6], [8]. Recently, several prototypes for extremely large array have been developed, such as the radio stripes [3] or extremely large RIS [8]. Moreover, extremely large arrays also offer opportunities for satellite, UAV, and offshore communications [9], [10]. On the other hand, benefiting from the enormous spectrum resource at millimeter wave (mmWave) or terahertz band (THz), high-frequency communications can provide a very wide bandwidth (e.g., several GHz) [11]. The very small size of high-frequency antennas also favorably enables the deployment of extremely large arrays [12]. Therefore, extremely large array for wideband communications is promising to support the ultra-high transmission rate for the next-generation communications [13].

A. Prior works

The change from large arrays to extremely large arrays not only means the increase in array aperture, but also leads to the fundamental change of the electromagnetic field property. The electromagnetic radiation field can be divided into two regions, i.e., the far-field region and the near-field region [14], [15]. In the far-field region, the channel is modeled under **planar wave** assumption, where the phase of array steering vector is *linear* to the antenna index [16]. By contrast, the near-field channel is modeled under **spherical wave** assumption, where the phase of array steering vector is *non-linear* to the antenna index [14]. The boundary between the near-field and far-field is determined by the Rayleigh distance [17], which is proportional to the square of the array aperture and inversely proportional to the wavelength. In current communications, since the array aperture is not very large, the near-field range is negligible. In this case, the classical beamforming techniques generate planar wavefront beams transmitting towards desired directions. However, as the antenna number increases dramatically in extremely

large array, the near-field range will expand by orders of magnitude. Typically, the Rayleigh distance of extremely large arrays can be up to several hundreds of meters, which covers a large part of a cell. In this case, the expected near-field beamforming should generate spherical wavefront beams to focus the beam energy around the desired location [18], which is decided by both direction and distance. By considering the non-negligible near-field range, near-field communications will be essential for the next-generation communications.

Moreover, when it comes to mmWave or THz wideband systems, the large antenna array prefer to utilize phased array [19], which can only realize *frequency-independent* narrowband beamforming. Due to the extremely large bandwidth, the generated beam wavefronts at different frequencies will deviate from that at the central frequency, which is called as the beam split effect [20]. Specifically, in the far-field, the beam split effect will result in the fact that beams at different frequencies split towards different directions [21], which is similar to the rainbow caused by the dispersion of white light [22]. However, in the near-field, the beam split effect will result in a new phenomenon that the beam energy at different frequencies focus on different locations, and thus the energy fail to focus on the desired receiver location. Consequently, only the beams around the central frequency can be received by the receiver, while most of the other beams will suffer from a serious array gain loss. Typically, more than 50% frequencies will suffer more than 60% array gain loss caused by the near-field beam split effect.

As the array aperture is not very large in current systems, existing works focus on solving the far-field beam split. The corresponding solutions can be generally classified into two categories, i.e., the algorithm design method and the hardware structure design method. For the first category solutions, by carefully optimizing the phase shifts (PSs) of phased array, wide beams can be generated to alleviate the beam split effect [20], [23]–[25]. However, since these methods either heavily depend on the linear phase property of array steering vector in the far-field region [20], [23], or assume the bandwidth is not very large [24], [25], they are not valid for near-field wideband systems. For the second category solutions, they adopt the large time-delay (TD) array rather than the classical phased array to generate *frequency-dependent* beams, which can nearly eliminate the beam split effect [26], [27]. Unfortunately, a large number of TDs will introduce much higher power consumption than PSs. Thus, it is impractical to deploy a large TD array [27]. To our best knowledge, the near-field beam split effect has not been well studied in the literature and there are no practical solutions so far.

B. Our contributions

In this paper, we propose a phase-delay focusing (PDF) method to address the near-field beam split problem. Our key contributions are summarized as follows.

- We first reveal the near-field beam split effect for extremely large antenna array, and then analyze the corresponding array loss caused by it.
- Then, to cope with this array gain loss, we first propose a piecewise-far-field model to approximate the near-field model with high accuracy in a piecewise-linear manner, where the entire large array is partitioned into multiple small sub-arrays. In this way, the receiver locates in the far-field region of a small sub-array but the near-field region of the entire large array. Inspired by this piecewise-far-field model, we insert a time-delay (TD) unit between the PSs and the radio-frequency (RF) chain in each sub-array. Then, through joint control of delay and phase, a PDF method is proposed to effectively mitigate the near-field beam split effect.
- Furthermore, from the perspective of array gain loss, a metric called effective Rayleigh distance is defined to distinguish the far-field and near-field. Compared to the classical Rayleigh distance defined from the perspective of phase error, effective Rayleigh distance is a more accurate metric for practical communications.
- Finally, theoretical and simulation results are provided to validate the proposed PDF method, which can mitigate the near-field beam split effect with near-optimal rate performance.

C. Organization and notation

Organization: The remainder of this paper is organized as follows. In section II, the system model is introduced, and the near-field beam split effect is revealed. In section III, the piecewise-far-field channel model and the PDF method are proposed. In section IV, we provide theoretical results to validate the proposed PDF scheme. Specifically, array gain performance is analyzed in section IV-A, the effective Rayleigh distance is derived in IV-B, and the sub-array antenna number is designed in IV-C. Simulations are carried out in Section V, and finally conclusions are drawn in Section VI.

Notation: Lower-case and upper-case boldface letters represent vectors and matrices, respectively; $X_{p,q}$ denotes the (p, q) -th entry of the matrix \mathbf{X} ; $\mathbf{X}_{p,:}$ and $\mathbf{X}_{:,p}$ denote the p -th row and the p -th column of the matrix \mathbf{X} ; $[\mathbf{a}]_n$ denotes the n -th element of the vector \mathbf{a} ; $(\cdot)^T$ and $(\cdot)^H$ denote the transpose and conjugate transpose, respectively; $|\cdot|$ denotes the absolute operator;

$\text{Tr}(\cdot)$ denotes the trace operator; $\mathcal{CN}(\mu, \Sigma)$ and $\mathcal{U}(a, b)$ denote the Gaussian distribution with mean μ and covariance Σ , and the uniform distribution between a and b , respectively.

II. NEAR-FIELD BEAM SPLIT

In this section, we will reveal the near-field beam split effect in wideband extremely large array systems. We suppose the base station (BS) is deployed with an N -element uniform linear array¹. Note that practical implementations for such extremely large linear array structure, namely radio stripes, has been proposed recently [3]. We denote $d = \frac{\lambda_c}{2}$, λ_c , c , $f_c = \frac{c}{\lambda_c}$, B , and M as the antenna spacing, carrier wavelength, light speed, central carrier, bandwidth, and number of sub-carriers, respectively. The coordinate of the n -th BS antenna is $(0, nd)$, $n = -\frac{N-1}{2}, \dots, \frac{N-1}{2}$, thus the array aperture is $D = N(d - 1) \approx Nd$. A single-antenna receiver is located at (x, y) , where its corresponding polar coordinate is $(r, \theta) = \left(\sqrt{x^2 + y^2}, \arctan \frac{y}{x}\right)$. Then, the line-of-sight near-field channel $\mathbf{h}(x, y, f_m) \in \mathbb{C}^{1 \times N}$ is modeled under spherical wave assumption [14] as

$$[\mathbf{h}(x, y, f_m)]_n = \sqrt{\beta(f_m)} \frac{e^{-j2\pi f_m \frac{r_n}{c}}}{r_n}, \quad (1)$$

where $[\mathbf{h}(x, y, f_m)]_n$ denotes the channel of the n -th antenna, f_m denotes the m -th sub-carrier, $\frac{\beta(f_m)}{r_n^2} = \left(\frac{c}{4\pi f_m r_n}\right)^2$ denotes the free-space path loss [28], and $r_n = \sqrt{x^2 + (y - nd)^2}$ denotes the distance between the n -th antenna and the receiver.

For the traditional phase-shifters (PSs) based beamforming, since it can only realize frequency-independent phase control [1], the commonly used near-field beamforming vector $\mathbf{w}(x, y) \in \mathbb{C}^{N \times 1}$ is determined by the channel at the central carrier f_c [18], i.e.,

$$[\mathbf{w}(x, y)]_n = \frac{1}{\sqrt{N}} \arg([\mathbf{h}(x, y, f_c)]_n^*) = \frac{1}{\sqrt{N}} e^{j2\pi f_c \frac{r_n}{c}}, \quad (2)$$

where $\arg(x)$ denotes the phase of x . Note that the phase $2\pi f_m \frac{r_n}{c}$ in (1) or (2) is non-linear to the antenna index n . Traditionally, since the array aperture is not very large, the far-field model under planar wave assumption is widely adopted to simplify this non-linear phase [16], i.e.,

$$2\pi \frac{f_m}{c} r_n - 2\pi \frac{f_m}{c} r \approx -2\pi \frac{f_m}{c} (n - 1)d \sin \theta. \quad (3)$$

It is clear in (3) that in the far-field, the phase $-2\pi \frac{f_m}{c} (n - 1)d \sin \theta$ is linear to the antenna index n , and the far-field beamforming weight $[\mathbf{w}(x, y)]_n = \frac{1}{\sqrt{N}} e^{-j2\pi \frac{f_c}{c} (n - 1)d \sin \theta}$ is only related to the

¹For expression simplicity, we consider the uniform linear array as an example in this paper. Note that the proposed scheme can be directly applied to other array types, such as uniform planar arrays.

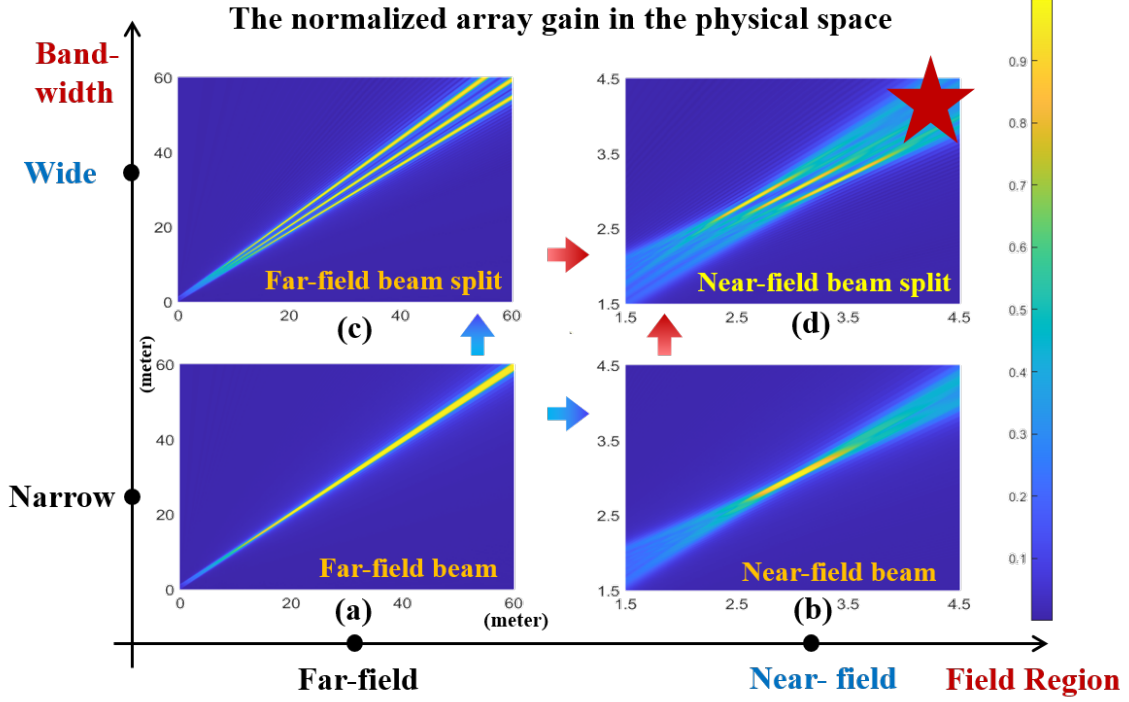


Fig. 1. This figure plots the normalized array gain in the physical space. We consider four scenarios: (a) the far-field narrowband scenario, (b) the near-field narrowband scenario, (c) the far-field wideband scenario, and (d) the near-field wideband scenario. In each sub-figure, the beam energy of the lowest, the central, and the highest frequencies are plotted (e.g., the three lines in the sub-figure (c) and (d)). Existing works mainly focus on the cases (a)(b)(c), while case (d) has not been studied yet.

direction θ . In this case, as shown in Fig. 1 (a), the generated beam will transmit signals towards the desired direction θ . However, since the linear phase approximation in (3) is not accurate when n is very large, the above far-field assumption does not hold anymore for an extremely large array. The near-field range is determined by the Rayleigh distance [28] $R = \frac{2D^2}{\lambda_c} = \frac{1}{2}N^2\lambda_c$, where $D = Nd$ denotes the array aperture. If the antenna number N increases dramatically, the near-field region will expand by orders of magnitude. For instance, if the antenna number 512 and the carrier is 100 GHz, then the Rayleigh distance is about 400 meters. In this case, the accurate spherical wave assumption has to be considered for the channel model $\mathbf{h}(x, y, f_m)$ in (1) and the corresponding beamforming $\mathbf{w}(x, y)$ in (2). Accordingly, as shown in Fig. 1 (b), the generated near-field beams is able to focus the beam energy around the desired location (r, θ) [29], which depends on both the distance and direction of the receiver.

The discussion above assume that the bandwidth is not very large, while when it comes to wideband systems, the beam split effect will be induced. We define $g(x', y', x, y, f_m) = |\mathbf{h}(x', y', f_m)\mathbf{w}(x, y)|$ as the array gain at frequency f_m on the location (x', y') with $r'_n =$

$\sqrt{x'^2 + (y' - nd)^2}$, where the beamforming vector is $\mathbf{w}(x, y)$. Then, we have

$$g(x, y, x', y', f_m) = \sqrt{\frac{\beta(f_m)}{N}} \left| \sum_{n=-\frac{N-1}{2}}^{\frac{N-1}{2}} \frac{1}{r'_n} e^{-j\frac{2\pi}{c}(f_m r_n - f_c r'_n)} \right|. \quad (4)$$

When $f_m \approx f_c$ in narrowband systems, the array gain $g(x', y', x, y, f_m)$ reaches its peak when $(x', y') = (x, y)$, which means that the beam energy is exactly focused on the location (x, y) . However, if $f_m \neq f_c$ in wideband systems, when $(x', y') = (x, y)$, the phase of the n -th element in (4) becomes $e^{-j\frac{2\pi}{c}(f_c - f_m)r_n}$. Since the phase $e^{-j\frac{2\pi}{c}(f_c - f_m)r_n}$ changes with the antenna index n , the array gain $g(x, y, x, y, f_m)$ at the frequency f_m will be significantly reduced. That is to say, the beam energy at f_m is split from the desired location (x, y) . In the far-field, where the distance is large, as shown in Fig. 1 (c), this beam split effect causes beams at different frequencies to split towards different directions [30]. However, in the near-field, as shown in Fig. 1 (d), the beam split effect will lead to the result that beams at different frequencies focus on different locations, and thus the receiver can only receive signals around the central frequency. For example, when we consider $f_c = 100$ GHz, $B = 5$ GHz and $N = 512$, due to the near-field beam split effect, more than 50% sub-carriers will suffer at least 60% array gain loss, which is not acceptable. Existing recent works mainly focus on mitigating the far-field beam split effect, they either deploy a large number of high power consumption devices, or heavily rely on the linear phase property of the far-field channel, which are not valid in the near-field. To our best knowledge, the non-negligible near-field beam split effect has not been studied in the literature.

III. PROPOSED METHODS

In this section, a piecewise-far-field channel with piecewise-linear phase is proposed to approximate the near-field channel at first, based on which we propose a phase-delay focusing (PDF) method to mitigate the near-field beam split effect.

A. Piecewise-far-field channel model

Due to the non-linear phase $-2\pi f_m \frac{r_n}{c}$ against the antenna index n as shown in (1), it is intractable to get a close form of the array gain $g(x', y', x, y, f_m)$ in (4), which makes it difficult to directly design near-field wideband beamforming. To simplify this non-linear phase with acceptable accuracy, we observe that the Rayleigh distance $\frac{1}{2}N^2\lambda_c$ is proportional to the square of antenna number, which means fewer antennas leads to better accuracy for the far-field assumption

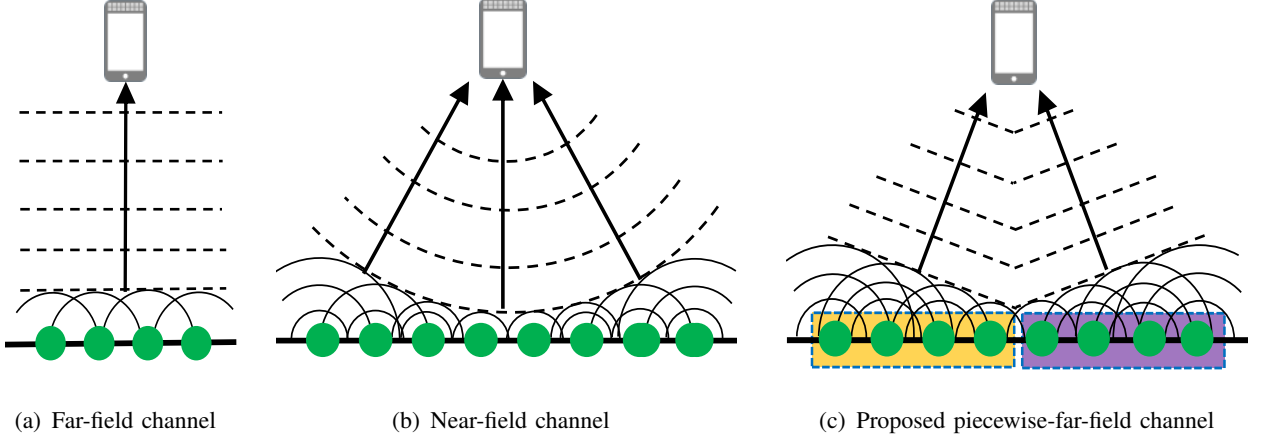


Fig. 2. Schematic diagrams of (a) far-field channel model, (b) near-field channel model, and (c) piecewise-far-field channel model.

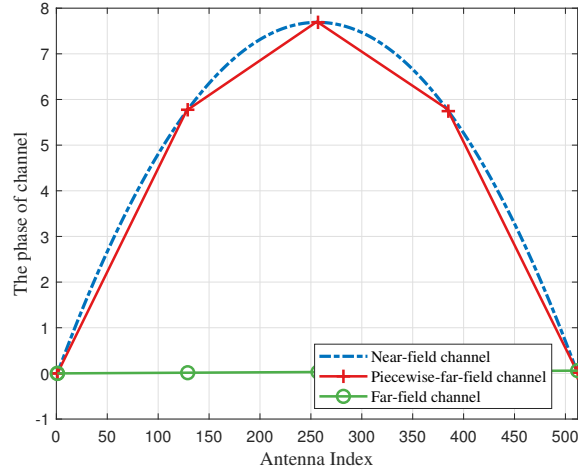


Fig. 3. This figure plots the channel phase against antenna index. The antenna number is 512, the carrier frequency is 100 GHz. The user is located at $(x, y) = (20 \text{ m}, 0 \text{ m})$. With $K = 4$ sub-arrays, the piecewise-far-field channel model can well approximate the near-field channel model.

in (3). Inspired by this observation, as shown in Fig. 2 (a)-(c), we propose a piecewise-far-field channel model to approximate the near-field channel model. In the proposed model, the entire large array is partitioned into multiple small sub-arrays, where the antenna number of each sub-array is much smaller than that of the entire array. With much fewer antennas, the near-field range of each sub-array can be negligible. Therefore, we can approximately suppose that the receiver locates in the near-field region of the entire large array, but in the far-field region of each sub-array.

Specifically, we divide the entire large array into K sub-arrays. For each sub-array, there are P adjacent antennas, so the total antenna number N is equal to KP . We ignore the term (x, y)

in $\mathbf{h}(x, y, f_m)$ for simplicity. Then, the near-field channel is rearranged as

$$\mathbf{h}(f_m) = \sqrt{\beta(f_m)} \left[\mathbf{h}_m^{(-\frac{K-1}{2})}, \mathbf{h}_m^{(-\frac{K+1}{2})}, \dots, \mathbf{h}_m^{(\frac{K-1}{2})} \right], \quad (5)$$

where $\mathbf{h}_m^{(k)} \in \mathbb{C}^{1 \times P}$ is the sub-channel between the k -th sub-array and the receiver. Denote the distance between the p -th antenna in the k -th sub-array and the receiver as $r_{k,p} = r_{kP+p}$, where $k \in \{-\frac{K-1}{2}, \dots, \frac{K-1}{2}\}$ and $p \in \{-\frac{P-1}{2}, \dots, \frac{P-1}{2}\}$. Then for the k -th sub-array, since the sub-array aperture is much smaller than the entire array aperture, the near-field channel $\mathbf{h}_m^{(k)}$ can be approximated by a far-field channel $\tilde{\mathbf{h}}_m^{(k)}$ as

$$[\mathbf{h}_m^{(k)}]_p = \frac{e^{-j2\pi f_m \frac{r_{k,p}}{c}}}{r_{k,p}} \approx \frac{e^{-j2\pi f_m L_k/c}}{L_k} e^{j\pi \eta_m p \sin \theta_k} = [\tilde{\mathbf{h}}_m^{(k)}]_p, \quad (6)$$

where $\eta_m = \frac{f_m}{f_c}$, $L_k = r_{k,0}$ and $\theta_k = \arccos\left(\frac{x}{L_k}\right)$ denote the distance and direction between the midpoint of the k -th sub-array and the receiver, respectively. Note that (6) can be directly derived by setting $r = L_k$ and $\theta = \theta_k$ in (3). In this way, the entire near-field channel can be approximated as the proposed piecewise-far-field channel model:

$$\mathbf{h}(f_m) \approx \tilde{\mathbf{h}}(f_m) = \sqrt{\beta(f_m)} \left[\tilde{\mathbf{h}}_m^{(-\frac{K-1}{2})}, \tilde{\mathbf{h}}_m^{(-\frac{K+1}{2})}, \dots, \tilde{\mathbf{h}}_m^{(\frac{K-1}{2})} \right]. \quad (7)$$

To illustrate the accuracy of the proposed model, in Fig. 3, we compare the channel phase against antenna index for the near-field, far-field and piecewise-far-field channel models. The phase of the piecewise-far-field channel model can accurately approximate the near-field channel. Furthermore, the proposed piecewise-far-field channel model can be regarded as a piecewise-linearization of the existing near-field channel model, i.e., in each sub-array, the phase is linear to the antenna index. Utilizing this piecewise-linear phase property, we will design a near-field wideband beamforming method named phase-delay focusing (PDF) to alleviate the near-field beam split in the next subsection.

B. Proposed phase-delay focusing scheme

Based on the proposed piecewise-far-field channel model above, the approximate channel phase in (6) can be decoupled into two parts: the first part is the near-field channel phase $-2\pi f_m \frac{L_k}{c}$ across different sub-arrays, and the second part is the far-field channel phase $\pi \eta_m p \sin \theta_k$ within each sub-array. Both of these two parts will contribute to the near-field beam split effect. However, since the antenna number of a sub-array is much smaller than that of the entire array, and the performance degradation caused by beam split is negligible when the antenna number is small

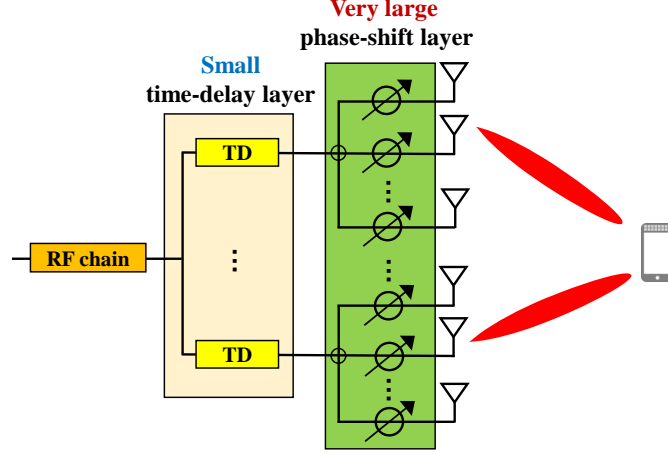


Fig. 4. Hardware architecture for the phase-delay focusing scheme to alleviate the near-field beam split effect.

[20], [31], we can derive that the far-field channel phase $\pi\eta_m p \sin \theta_k$ has little effect on the near-field beam split. Thus, our task is turned to compensate for the near-field channel phase $-2\pi f_m \frac{L_k}{c}$ to alleviate the near-field beam split effect across different sub-arrays.

Note that the channel phase $-2\pi f_m \frac{L_k}{c}$ is linear to the frequency f_m , which can be realized by the time delay of $\frac{L_k}{c}$. Therefore, to compensate for the phase $-2\pi f_m \frac{L_k}{c}$ across different sub-arrays, as shown in Fig. 4, in each sub-array, we insert one time-delay (TD) unit between the radio-frequency (RF) chain and the phase shifters (PSs). Since the frequency response of TD is $e^{-j2\pi f\tau}$, where τ is the actual time delay, it can exactly compensate for the phase $-2\pi f_m \frac{L_k}{c}$ when $\tau = -\frac{L_k}{c}$. Moreover, as shown in Fig. 4, the main function of the PSs is to generate far-field planar waves to match the far-field phase $\pi\eta_m p \sin \theta_k$ within each sub-array. Through the joint control of phase and delay, the beam energy across the entire bandwidth can be approximately focused on the receiver location (x, y) , thus we call this method as phase-delay focusing (PDF).

It is worth noting that the hardware architecture in Fig. 4 has also been utilized in [20] to deal with the far-field beam split effect. However, since the directions θ_k and distances L_k of different sub-arrays are assumed to be the same in [20], the beamforming method proposed in [20] can not address the near-field beam split problem. Moreover, since the TD number is much less than the antenna number, the power consumption of the TD layer is much smaller than that of the traditional massive TD arrays [31].

In the following discussions, we elaborate on the proposed PDF method. Since the TD number is equal to the sub-array number K , the wideband beamforming vector \mathbf{w}_m at frequency f_m

realized by the proposed PDF method is composed of K sub-vectors, i.e.,

$$\mathbf{w}_m = \frac{1}{\sqrt{N}} \left[\mathbf{w}_m^{(-\frac{K-1}{2})^T}, \mathbf{w}_m^{(-\frac{K+1}{2})^T}, \dots, \mathbf{w}_m^{(\frac{K-1}{2})^T} \right]^T, \quad (8)$$

where $\mathbf{w}_m^{(k)} \in \mathbb{C}^{P \times 1}$ denotes the beamforming vector of the k -th sub-array. As shown in Fig. 4, $\mathbf{w}_m^{(k)}$ is generated by one TD unit and P PSs, which can be expressed as

$$[\mathbf{w}_m^{(k)}]_p = e^{-j2\pi f_m t_k} e^{j\pi p \beta_k}. \quad (9)$$

It is clear from (9) that $\mathbf{w}_m^{(k)}$ is composed of two parts. The first part is the frequency-independent phase $\pi p \beta_k$ realized by P phase shifters in the k -th sub-array, while the second part is the frequency-dependent phase $-2\pi f_m t_k$ realized by the k th TD unit. As discussed before, $\pi p \beta_k$ is designed to generate planar waves to match the far-field phase $\pi \eta_m p \sin \theta_k$, while TD t_k is designed to compensate for the near-field phase $-2\pi f_m \frac{L_k}{c}$. In the other words, The optimal delay t_k and phase β_k to be designed for the proposed PDF method is to maximize the array gain across the entire bandwidth to focus the beam energy on the desired location (x, y) . Specifically, the array gain achieved by the proposed PDF method is written as

$$\begin{aligned} \mathbf{h}(f_m) \mathbf{w}_m &\approx \tilde{\mathbf{h}}(f_m) \mathbf{w}_m = \sqrt{\frac{\beta(f_m)}{N}} \sum_{k=-\frac{K-1}{2}}^{\frac{K-1}{2}} \tilde{\mathbf{h}}_m^{(k)} \mathbf{w}_m^{(k)} \\ &= \sqrt{\frac{\beta(f_m)}{N}} \sum_{k=-\frac{K-1}{2}}^{\frac{K-1}{2}} \frac{1}{L_k} e^{-j2\pi f_m (t_k + \frac{L_k}{c})} \sum_{p=-\frac{P-1}{2}}^{\frac{P-1}{2}} e^{jp\pi(\beta_k + \eta_m \sin \theta_k)}. \end{aligned} \quad (10)$$

To generate planar waves matching the sub-array channel, β_k realized by the PSs is usually designed according to the central carrier spatial direction $\sin \theta_k$ [32], i.e.,

$$\beta_k^* = -\phi_k = -\sin \theta_k, \quad (11)$$

where we set $\phi_k = \sin \theta_k$. By substituting (11) into (10), we obtain

$$\tilde{\mathbf{h}}_m^{(k)} \mathbf{w}_m^{(k)} = \frac{1}{L_k} e^{-j2\pi f_m (t_k + \frac{L_k}{c})} \Xi_P((1 - \eta_m) \phi_k), \quad (12)$$

where $\Xi_P(x) = \frac{\sin(\frac{P}{2}\pi x)}{\sin(\frac{1}{2}\pi x)}$. The PDF method aims to design t_k to maximize the array gain across the entire bandwidth to focus the beam energy on the desired location (x, y) . Thus, the corresponding optimization problem can be formulated as

$$\begin{aligned} &\underset{\{t_k\}}{\text{maximize}} \quad \sum_{m=1}^M \left| \sum_{k=-\frac{K-1}{2}}^{\frac{K-1}{2}} \tilde{\mathbf{h}}_m^{(k)} \mathbf{w}_m^{(k)} \right| \\ &\text{s.t.} \quad t_k \geq 0 \quad k \in \{1, 2, \dots, K\}. \end{aligned} \quad (13)$$

We give out the following **Lemma 1** to solve the optimization problem (13) above.

Lemma 1: Define $(1 - \eta_m)\phi_k$ as the direction deviations at the frequency f_m . If all of the direction deviations are within the main lobe of $\Xi_P(\cdot)$, which means $|(1 - \eta_m)\phi_k| \leq |1 - \eta_m| < \frac{2}{P}, \forall m \in \{1, 2, \dots, M\}$, then the optimal solution to optimization problem (13) is

$$t_k^* = T - \frac{L_k}{c}, \quad (14)$$

where T is a common delay to guarantee $\min\{t_k^*\} \geq 0$.

Proof: By substituting (14) into (12), the array gain of the k -th sub-array is rewritten as

$$\tilde{\mathbf{h}}_m^{(k)} \mathbf{w}_m^{(k)} = \frac{1}{L_k} e^{-j2\pi f_m T} \Xi_P((1 - \eta_m)\phi_k). \quad (15)$$

Since all of the direction deviations $(\eta_m - 1)\phi_k$ across the entire wideband are within the main lobe of $\Xi_P(\cdot)$, which means $|(\eta_m - 1)\phi_k| \leq |\eta_m - 1| < \frac{2}{P}$, then it is obvious that $\Xi_P((\eta_m - 1)\phi_k) > 0$. Note that as the antenna number of a sub-array P is much smaller than that of the entire array N , the assumption that $|\eta_m - 1| < \frac{2}{P}$ is rational. Note that in section IV, we will further discuss how to design the sub-array antenna number P . In this case, the array gain can be rewritten as

$$\left| \sum_k \tilde{\mathbf{h}}_m^{(k)} \mathbf{w}_m^{(k)} \right| = \sum_k \frac{1}{L_k} \Xi_P((1 - \eta_m)\phi_k). \quad (16)$$

In addition, based on the Cauchy-Schwarz inequality, we can derive the upper bound of the array gain as

$$\left| \sum_k \tilde{\mathbf{h}}_m^{(k)} \mathbf{w}_m^{(k)} \right| \leq \sum_k \left| \tilde{\mathbf{h}}_m^{(k)} \mathbf{w}_m^{(k)} \right| = \sum_k \frac{1}{L_k} \Xi_P((1 - \eta_m)\phi_k). \quad (17)$$

It is clear from (16) and (17) that t_k^* is the optimal solution to $\left| \sum_k \tilde{\mathbf{h}}_m^{(k)} \mathbf{w}_m^{(k)} \right|$ at the frequency f_m . Moreover, since $t_k^* = T - \frac{L_k}{c}$ is frequency-independent, it is the optimal solution to all sub-carriers. Therefore, t_k^* is the optimal solution to problem (13), which completes the proof. ■

To sum up, (11) and (14) complete the design of the proposed PDF scheme². In the next section, we will provide theoretical analysis to verify the performance of the proposed PDF scheme.

²Recently, it has been experimentally shown to integrate an additional power amplifier for each RIS element [33]. To realize phase-delay focusing architecture on RIS, one can similarly integrate an additional time-delay unit for each sub-array of a RIS. Therefore, the proposed phase-delay focusing architecture can also be applied to the RIS aided communications.

IV. THEORETICAL ANALYSIS

In this section, we provide theoretical analysis to verify the effectiveness of the proposed PDF scheme. We firstly evaluate the achieved array gain of the PDF method. Then we derive a more accurate metric to distinguish the near-field region, namely effective Rayleigh distance. Finally, we elaborate on how to design the antenna number of each sub-array.

A. The achieved array gain of the proposed PDF method

To better understand whether the proposed PDF method can mitigate the near-field beam split effect, we will derive the normalized array gain achieved by the proposed PDF method across the entire wideband.

For comparison, we first give out the optimal near-field wideband beamforming vector $\mathbf{w}_m^{\text{opt}} \in \mathbb{C}^{N \times 1}$ realized by the massive TD array, i.e.,

$$[\mathbf{w}_m^{\text{opt}}]_n = \frac{1}{\sqrt{N}} e^{j2\pi f \tau_n}, \quad (18)$$

The wideband beamforming vector in (18) can completely eliminate the near-field beam split effect [26]. However, since the cost and power consumption of TD are much higher than phase shifter (PS) [20], it is not practical to deploy a massive TD array. We just regard it as an ideal case for comparison. The array gain at the m th sub-carrier achieved by $\mathbf{w}_m^{\text{opt}}$ is

$$g_m^{\text{opt}} = |\mathbf{h}(f_m) \mathbf{w}_m^{\text{opt}}| = \sqrt{\frac{\beta(f_m)}{N}} \sum_{n=-\frac{N-1}{2}}^{\frac{N-1}{2}} \frac{1}{r_n}, \quad (19)$$

which represents the performance upper bound of the ideal wideband array achieved by massive TD array. Then, by adopting the solutions of β_k^* , t_k^* derived in section III, the approximate normalized array gain can be obtained based on the following **Lemma 2**.

Lemma 2: If the user is located in the far-field region of a sub-array and all of the direction deviations $(\eta_m - 1)\phi_k$ are within the main lobe of $\Xi_P(\cdot)$, i.e., $|(\eta_m - 1)\phi_k| \leq |\eta_m - 1| < \frac{2}{P}$, $\forall m \in \{1, 2, \dots, M\}$, then the normalized array gain achieved by the proposed PDF method can be approximated as

$$\frac{g_m}{g_m^{\text{opt}}} \approx \frac{\Xi_P(1 - \eta_m)}{P} + \frac{P - \Xi_P(1 - \eta_m)}{P} \frac{\sum_k \frac{x_k^2}{L_k^3}}{\sum_k \frac{1}{L_k}}, \quad (20)$$

where $g_m = |\mathbf{h}(f_m) \mathbf{w}_m|$ denotes the array gain achieved by the PDF method.

Proof: See Appendix A. ■

From **Lemma 2**, some conclusions can be derived. Since $\frac{x}{L_k} = \cos \theta_k$, it is observed from (20) that

$$\frac{\sum_k \frac{x^2}{L_k^3}}{\sum_k \frac{1}{L_k}} = \frac{\sum_k \frac{\cos^2 \theta_k}{L_k}}{\sum_k \frac{1}{L_k}} \geq \min_{\theta_k} \{\cos^2 \theta_k\}. \quad (21)$$

We denote $\xi = \min_{\theta_k} \{\cos^2 \theta_k\}$, and then by combining (20) and (21), we can obtain the lower bound of the normalized array gain as

$$\frac{g_m}{g_m^{\text{opt}}} \geq g_m^{\text{LB}} = (1 - \xi) \frac{\Xi_P(1 - \eta_m)}{P} + \xi. \quad (22)$$

The lower bound in (22) solely depends on the sub-array antenna number P , rather than the entire antenna number N . This observation confirms that by inserting one TD into each sub-array, the near-field beam split among different sub-arrays is effectively eliminated. Meanwhile, the sole array gain loss term $\Xi_P(1 - \eta_m)/P$ is caused by the near-field beam split within each sub-array. Since P is much smaller than the entire antenna number N , the near-field beam split within each sub-array is slight and acceptable. For instance, if the bandwidth B is 5 GHz, the carrier frequency f_c is 100 GHz, then the maximum $|\eta_m - 1|$ is $\frac{B}{2f_c} = 0.025$. For a 512-antenna array, if we divide this array into $K = 16$ sub-arrays, then the antenna number of a sub-array is $P = 32$. By assuming that the typical sector range of a BS is $[-\frac{\pi}{3}, \frac{\pi}{3}]$, we can approximately obtain $\xi = \min_{\theta_k} \{\cos^2 \theta_k\} = \cos^2 \frac{\pi}{3} = \frac{1}{4}$. Based on the parameters above, the lower bound g_m^{LB} is larger than 0.82 according to (22), which means the array gain loss is less than 18% across the entire wideband. Thus we can conclude that the near-field beam split effect is effectively alleviated.

B. The proposed effective Rayleigh distance

In the previous sections, we assume the user is located in the far-field range of a sub-array, but in the near-field range of the entire array. Therefore, it is essential to identify the near-field range of a sub-array and the entire array. As we have mentioned before, it is a standard way to utilize the Rayleigh distance to calculate the near-field range. However, in our simulations, we observe that the Rayleigh distance overestimate the actual near-field range. For example, when the antenna number is $N = 512$, and the carrier is $f_c = 100$ GHz, the Rayleigh distance is around 400 meters, but the far-field method DPP-TTD [20] will not suffer from an obvious rate loss until the distance is less than 120 meters, which will be shown in section V. This

observation implies that, the classical Rayleigh distance is not accurate to distinguish the near-field region when evaluating the transmission rate. Therefore, a more accurate metric to identify the near-field region is required to evaluate the transmission rate.

We first explain why the Rayleigh distance overestimates the near-field range. We denote the phase error between the far-field channel and near-field channel on the n -th antenna as $E_n = \frac{2\pi f}{c}r_n - \frac{2\pi f}{c}(r - nd \sin \theta)$. Then, the Rayleigh distance is defined as follows: if the distance between the receiver and the BS array is larger than the Rayleigh distance $R = \frac{2D^2}{\lambda}$, then the maximum allowable phase error $E = \max_n E_n$ is no more than $\frac{\pi}{8}$. That is to say, if the maximum phase error E is larger than $\frac{\pi}{8}$, then the receiver is in the near-field region. However, since the phase error does not directly impact the transmission rate, the Rayleigh distance is not accurate to distinguish the near-field and far-field when evaluating the transmission rate.

On the other hand, since the near-field effect directly impacts the array gain, and array gain directly determines the transmission rate, an intuitive idea is to define a new metric to distinguish the near-field from the perspective of array gain. Specifically, we define a new metric called effective Rayleigh distance. If the BS utilizes the classical far-field beam with planar wavefront to serve a user, when the corresponding normalized array gain is less than 95% (note that this threshold can be changed), then the user is in the near-field, otherwise, the user is in the far-field. This new boundary to divide the near-field and far-field regions is the effective Rayleigh distance.

In the following discussions, we approximately derive the close form of the proposed effective Rayleigh distance. As mentioned before, if the receiver location is (r, θ) , the near-field beamforming vector at frequency f should be

$$[\mathbf{w}_N(r, \theta)]_n = \frac{1}{\sqrt{N}} e^{j2\pi f \frac{r_n}{c}}, \quad (23)$$

where $r_n = \sqrt{x^2 + (y - nd)^2} = \sqrt{r^2 - 2rnd \sin \theta + n^2 d^2}$. With the far-field approximation in (3), the far-field beamforming vector can be approximated as

$$[\mathbf{w}_F(\theta)]_n = \frac{1}{\sqrt{N}} e^{-j2\pi f \frac{nd \sin \theta}{c}}. \quad (24)$$

The definition of the effective Rayleigh distance indicates that, if the BS utilizes the far-field beamforming vector $\mathbf{w}_F(\theta)$ to transmit signals, only when the distance r is less than the effective Rayleigh distance R_{eff} , then the array gain $\mu(r, \theta) = |\mathbf{w}_F(\theta)^H \mathbf{w}_N(r, \theta)|$ will be smaller than 95%. Therefore, one can solve the equation $\mu(R_{\text{eff}}, \theta) = 95\%$ to derive the corresponding effective

Rayleigh distance R_{eff} . Based on this definition, we give out the following **Lemma 3** to calculate the effectively Rayleigh distance.

Lemma 3: Define the R_{eff} as the effective Rayleigh distance that the coherence $\mu(R_{\text{eff}}, \theta) = |\mathbf{w}_F(\theta)^H \mathbf{w}_N(R_{\text{eff}}, \theta)| = 95\%$, then the effectively Rayleigh distance R_{eff} can be obtained as

$$R_{\text{eff}} = \epsilon \cos^2 \theta \frac{2D^2}{\lambda}, \quad (25)$$

where $\epsilon = 0.367$.

Proof: See Appendix B. ■

It is obvious from (25) that, the effective Rayleigh distance is less than the Rayleigh distance, and it is also related to the direction θ . Since the effective Rayleigh distance is defined from perspective of the array gain that directly affects the transmission rate, it is a more accurate metric to determine the near-field range for practical communications. In section V, the accuracy of the effective Rayleigh distance will be verified, e.g., the existing far-field beamforming scheme [20] will actually suffer from an obvious rate loss when the distance is exactly less than the effective Rayleigh distance.

C. Design the antenna number of a sub-array

In this subsection, we utilize the conclusions derived in the previous two subsections to design the sub-array antenna number P , which is the most important design parameter of the proposed PDF method. Firstly, to satisfy the assumptions in **Lemma 1**, all of the direction deviations should be smaller than $\frac{2}{P}$, so we have $\max |\eta_m - 1| = \max \left| \frac{f_m}{f_c} - 1 \right| = \frac{B}{2f_c} \leq \frac{2}{P}$. Then, according to **Lemma 2**, the receiver should be located in the far-field region of each sub-array, where the array aperture of a sub-array is $D' = D/K \approx Pd$. Define ρ as the minimum allowable distance between the receiver and the BS, then according to the effective Rayleigh distance provided in (25), we have $\rho \geq 0.367 \frac{2D'^2}{\lambda} \approx 0.183P^2\lambda$. Meanwhile, based on the lower bound of the array gain achieved by the PDF scheme derived in (22), if the minimum allowable array gain is γ , then $g_m^{\text{LB}} \geq \gamma$ should be satisfied.

In conclusion, according to the three requirements above, the sub-array antenna number P should satisfy

$$P \leq \min \left\{ \frac{4f_c}{B}, \sqrt{\frac{\rho}{0.183\lambda}}, P_\gamma \right\}, \quad (26)$$

where P_γ is obtained by solving the transcendental equation $g_m^{\text{LB}} = \gamma$ in (22). For instance, if the bandwidth and carrier are $B = 5$ GHz and $f_c = 100$ GHz, respectively. The sector range of

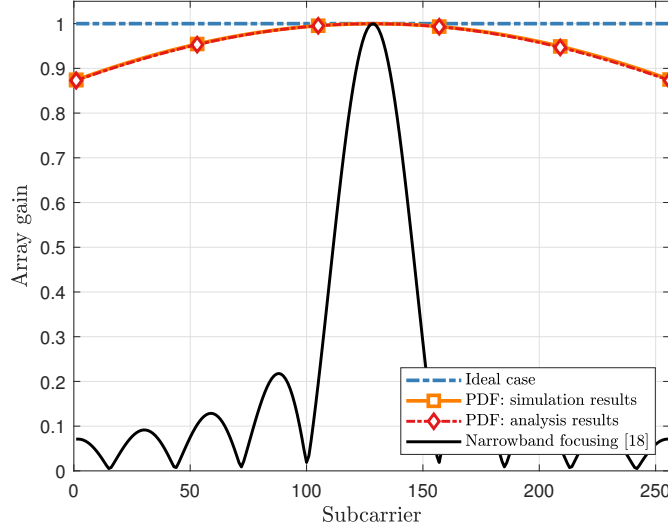


Fig. 5. Array gains among the entire working band. The blue line is realized by massive TD arrays representing the ideal case. The dotted lines indicate the analysis results shown in (20).

a BS is $[-\frac{\pi}{3}, \frac{\pi}{3}]$. The minimum distance ρ is 1 meter and the minimum allowable array gain γ is 80%. Then we have $\frac{4f_c}{B} = 80$, $\sqrt{\frac{\rho}{0.183\lambda}} \approx 43$ and $P_\gamma \approx 33$. Therefore, for the above typical system settings, the antenna number of a sub-array can be $P = 32$. This means if a 512-antenna array is deployed, then only $K = \frac{512}{32} = 16$ TDs are enough to alleviate the near-field beam split effect, which will be verified by simulation results in the next section.

V. SIMULATION RESULTS

In this section, simulation results are provided to verify the performance of the proposed PDF method. The central frequency and bandwidth are $f_c = 100$ GHz, $B = 5$ GHz, respectively. The number of sub-carriers M is 256. Without special statements, the antenna number N is 512, which can be implemented by radio stripes. As discussed in section IV-C, the number of sub-arrays is $K = 16$.

Fig. 5 shows the normalized array gains across the entire wideband. The user is located at $(r, \theta) = (10 \text{ m}, \frac{\pi}{4})$. The blue line is achieved by the massive TD array, which represents the ideal case for comparison [26]. The red dotted lines illustrate the theoretical results provided in (20). Firstly, for the traditional narrowband focusing method [18], there exist several deep fading points across the working band, so the signals at these sub-carriers cannot be transmitted. However, with 16 TDs, the proposed PDF method can effectively avoid these deep fading points. As we have mentioned in section IV-C, with $K = 16$ TDs, PDF method can achieve at least

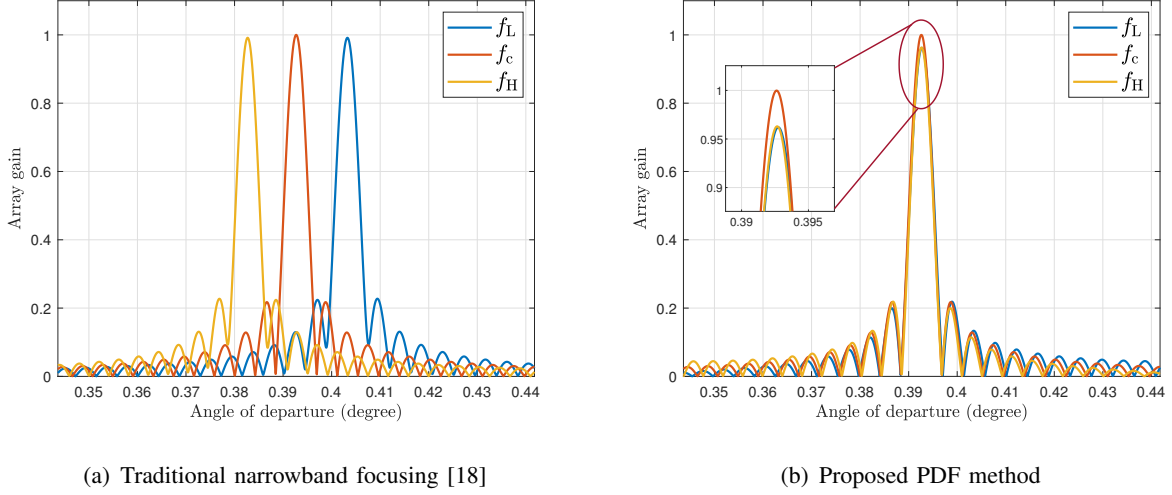


Fig. 6. Array gain performance against AoD with fixed distance.

80% ideal array gain performance over the entire wideband, the simulation results are consistent well with the analysis results.

Figs. 6 shows the array gain performance at different sub-carriers against the angle of departure (AoD) with a fixed distance. Fig. 6 (a) is for the traditional near-field narrowband focusing method [18], while Fig. 6 (b) is for the proposed PDF method. We use f_L , f_c , and f_H to denote the lowest, the central, and the highest frequency, respectively. We desire to focus the beam energy on the receiver location $(r, \theta) = (10 \text{ m}, \frac{\pi}{8})$. For the traditional narrowband focusing scheme [18], the near-field beam split effect makes the focused locations of the beams at f_L and f_H deviate from that at the central carrier f_c . However, the proposed PDF method can effectively focus the energy of beams at f_L and f_H at the desired receiver location, and the beams at f_L and f_H achieve more than 95% of the highest array gain at the desired location.

We further evaluate the average rate performance $C = \frac{1}{M} \sum_{m=1}^M \log_2 \left(1 + \frac{P_T}{\sigma^2} |\mathbf{h}(f_m) \mathbf{w}_m|^2 \right)$, where the transmit signal-to-noise ratio $\text{SNR} = \frac{P_T}{\sigma^2}$ is 25 dB. The average rate against the distance r is shown in Fig. 7. We compare the proposed PDF method with existing schemes, including the ideal case realized by massive TD array, narrowband focusing [18], optimization-based method [25], and the far-field beam split solution DPP-TTD [20]. To highlight the impact of the near-field effect, we ignore the large-scale path loss. The receiver moves from $(500 \text{ m}, \frac{\pi}{8})$ to $(0.5 \text{ m}, \frac{\pi}{8})$. The average rate of the proposed PDF scheme can always approach the ideal case with a rate loss less than 1%. It is worth noting that with 512 antenna elements at frequency

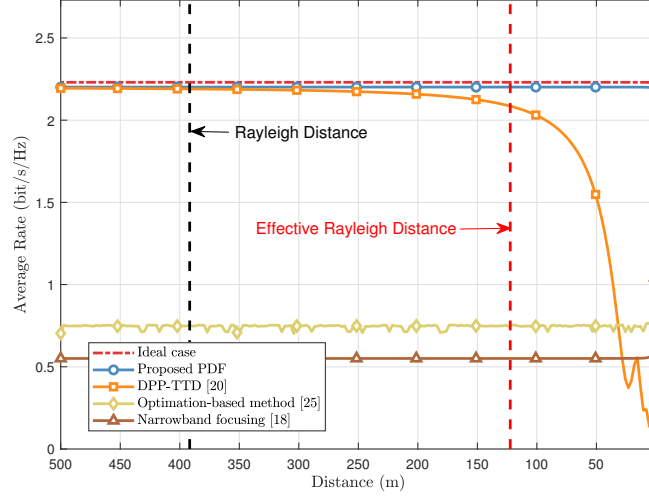


Fig. 7. Average rate against the distance. The antenna number is $N = 512$. The receiver is moving from $(r_1, \theta) = (500 \text{ m}, \frac{\pi}{8})$ to $(r_2, \theta) = (0.5 \text{ m}, \frac{\pi}{8})$ in a straight line.

$f_c = 100 \text{ GHz}$, the classical Rayleigh distance is around 400 meters. However, in Fig. 7, the far-field method DPP-TTD [20] will not suffer from an obvious rate loss until the distance is less than 120 meters, which implies when evaluating the achievable rate, the Rayleigh distance is not accurate to distinguish the far-field and near-field regions. This is because the Rayleigh distance is derived based on the phase error [17], which does not directly affect the achievable rate. As discussed in section IV-B, from the perspective of array gain, we define a new metric called effective Rayleigh distance to distinguish the near-field range. Since the array gain directly affect the achievable rate, the effective Rayleigh distance is a more accurate metric to identify the near-field range for practical communications. The average rate of the far-field method [20] actually becomes degraded when the distance is less than the effective Rayleigh distance, not the classical Rayleigh distance.

Finally, average rate against the number of BS antenna is shown in Fig. 8. The receiver is located at $(r, \theta) = (30 \text{ m}, \frac{\pi}{8})$. The antenna number is gradually increasing from 16 to 1024. The number of sub-arrays is fixed as $K = 16$, where the antenna number P of a sub-array is increasing from 1 to 64. As the BS antenna number increases, all existing schemes will suffer from a severe rate loss compared with the ideal case. However, the proposed PDF scheme can always achieve the near-optimal performance. Therefore, the near-field beam split effect is effectively alleviated.

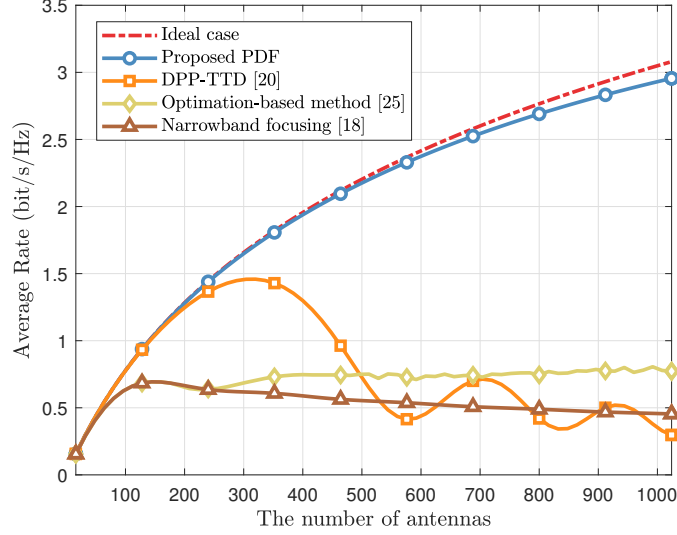


Fig. 8. Average rate against the total antenna number. The receiver is located at $(r, \theta) = (30 \text{ m}, \frac{\pi}{8})$. The number of sub-arrays is fixed as $K = 16$, and the antenna is gradually increasing from 16 to 1024.

VI. CONCLUSIONS

In this paper, we reveal an important challenge for future communications based on extremely large array, i.e., the near-field beam split. To address this challenge, we first propose a piecewise-far-field model to approximate the near-field channel with high accuracy, based on which we propose a PDF method through joint phase and delay control to significantly alleviate the near-field beam split effect. Moreover, we further define a new effective Rayleigh distance from the perspective of array gain, which is more accurate to distinguish the near-field range than the Rayleigh distance for practical communications. Finally, theoretical and numerical results are provided to demonstrate the effectiveness of our work. For future works, we may consider the near-field wideband channel estimation [34] or the near-field beam split effect in RIS-aided communications.

APPENDIX A. THE PROOF OF LEMMA 2

Referring to (16), the array gain g_m achieved by the proposed PDF method can be approximated as

$$g_m \approx \frac{c}{2\pi f_m \sqrt{N}} \sum_{k=-\frac{K-1}{2}}^{\frac{K-1}{2}} \frac{1}{L_k} \Xi_P((1 - \eta_m)\phi_k). \quad (27)$$

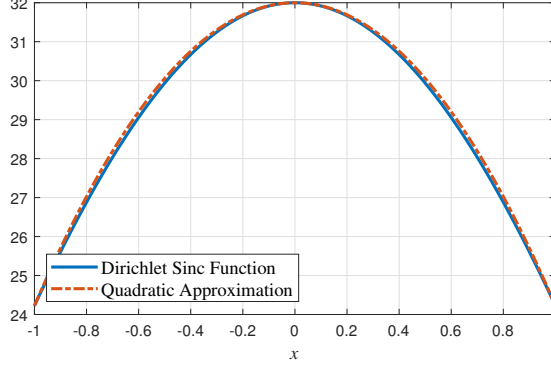


Fig. 9. Quadratic approximation $P - (P - \Xi_P(1 - \eta_m))x^2$ of the Dirichlet sinc function $\Xi_P((1 - \eta_M)x)$, where $x \in [-1, 1]$ and $P = 32$.

Since it is difficult to calculate the sum of the Dirichlet function, as shown in Fig. 9, we utilize a polynomial to fit the function $\Xi_P((1 - \eta_m)\phi)$ by three points $(-1, \Xi_P(1 - \eta_m))$, $(0, P)$, and $(1, \Xi_P(\eta_m - 1))$, then we have

$$\Xi_P((1 - \eta_m)\phi_k) \approx P - (P - \Xi_P(1 - \eta_m))\phi_k^2. \quad (28)$$

In this way, the normalized array gain is rewritten as

$$\frac{g_m}{g_m^{\text{opt}}} \approx \frac{\sum_{k=-\frac{K-1}{2}}^{\frac{K-1}{2}} \frac{P}{L_k}}{\sum_{n=-\frac{N-1}{2}}^{\frac{N-1}{2}} \frac{1}{r_n}} - \frac{P - \Xi_P(1 - \eta_m)}{P} \frac{\sum_{k=-\frac{K-1}{2}}^{\frac{K-1}{2}} \frac{P}{L_k} \phi_k^2}{\sum_{n=-\frac{N-1}{2}}^{\frac{N-1}{2}} \frac{1}{r_n}}. \quad (29)$$

Moreover, by referring to (19), the array gain $g_m^{\text{opt}} = \frac{c}{2\pi f_m \sqrt{N}} \sum_{n=1}^N \frac{1}{r_n}$ can be achieved by the optimal wideband beamforming realized by the massive TD array for the near-field channel. Similarly, we can regard $\frac{c}{2\pi f_m \sqrt{N}} \sum_k \frac{P}{L_k}$ as the array gain achieved by the optimal wideband beamforming for the piecewise-far-field channel. Since the user is located in the far-field region of a sub-array, the piecewise-far-field channel can well approximate the near-field channel, so we have

$$\sum_n \frac{1}{r_n} \approx \sum_k \frac{P}{L_k}. \quad (30)$$

Then, by substituting (30) into (29), we can obtain

$$\frac{g_m}{g_m^{\text{opt}}} \approx \frac{\Xi_P(1 - \eta_m)}{P} + \frac{P - \Xi_P(1 - \eta_m)}{P} \frac{\sum_k \frac{\phi_k}{L_k}}{\sum_k \frac{1}{L_k}} \quad (31)$$

$$= \frac{\Xi_P(1 - \eta_m)}{P} + \frac{P - \Xi_P(1 - \eta_m)}{P} \frac{\sum_k \frac{x^2}{L_k^3}}{\sum_k \frac{1}{L_k}}, \quad (32)$$

where $\phi_k^2 = \frac{x^2}{L_k^2}$. Therefore, the approximation (20) in **Lemma 2** is proved.

APPENDIX B. THE PROOF OF LEMMA 3

The coherence $\mu(r, \theta)$ can be expressed as

$$\mu(r, \theta) = \frac{1}{N} \left| \sum_{n=-\frac{N-1}{2}}^{\frac{N-1}{2}} e^{j2\pi \frac{f}{c} (r_n + nd \sin \theta)} \right|. \quad (33)$$

It is intractable to get a close-form solution of (33), so we approximate it by the second-order Taylor expansion of r_n , i.e., $r_n = \sqrt{r^2 - 2rnd \sin \theta + n^2 d^2} \stackrel{(a)}{\approx} r - nd \sin \theta + \frac{n^2 d^2 \cos^2 \theta}{2r}$, where (a) is derived based on $\sqrt{1+x} \approx 1 + \frac{1}{2}x - \frac{1}{8}x^2$. Then, (33) can be approximated as

$$\mu(r, \theta) \approx \frac{1}{N} \left| \sum_{n=-(N-1)/2}^{(N-1)/2} e^{j\pi \frac{f}{c} \frac{n^2 d^2 \cos^2 \theta}{r}} \right| = |F(x)|. \quad (34)$$

where $x = \frac{f d^2 \cos^2 \theta}{c r} = \frac{d^2 \cos^2 \theta}{\lambda r}$, and

$$F(x) = \frac{1}{N} \sum_{n=-(N-1)/2}^{(N-1)/2} e^{j\pi n^2 x} \approx \frac{1}{N} \int_{-N/2}^{N/2} e^{j\pi n^2 x} \mathrm{d}n. \quad (35)$$

Since $x = \frac{d^2 \cos^2 \theta}{\lambda r}$ is larger than 0, the function $F(x)$ can be rewritten as

$$\begin{aligned} F(x) &\approx \frac{2}{N} \int_0^{N/2} e^{j\pi n^2 x} \mathrm{d}n \stackrel{(a)}{=} \frac{2}{\sqrt{2xN}} \int_0^{\sqrt{2xN}/2} e^{j\frac{\pi}{2} t^2} \mathrm{d}t \\ &\stackrel{(b)}{=} \frac{C(y) + jS(y)}{y} = G(y), \end{aligned} \quad (36)$$

where $C(y) = \int_0^y \cos(\frac{\pi}{2} t^2) \mathrm{d}t$ and $S(y) = \int_0^y \sin(\frac{\pi}{2} t^2) \mathrm{d}t$ are the Fresnel functions. Note that (a) is derived by letting $n^2 x = \frac{1}{2} t^2$, and (b) is derived by letting $y = \frac{\sqrt{2xN}}{2}$. To sum up, combining (34), (35), and (36), we can approximate the coherence $\mu(r, \theta)$ as

$$\mu(r, \theta) \approx \left| G \left(\frac{\sqrt{2xN}}{2} \right) \right| = \left| G \left(\sqrt{\frac{N^2 d^2 \cos^2 \theta}{2\lambda r}} \right) \right| = |G(y)|, \quad (37)$$

where $y = \sqrt{\frac{N^2 d^2 \cos^2 \theta}{2\lambda}}$ and $G(y) = \frac{C(y) + jS(y)}{y}$. It is clear from (37) that the coherence heavily relies on the property of the function $G(y)$. Fortunately, $G(y)$ does not contain any parameters, thus it is sufficient to obtain its numerical result by offline integration.

As shown in Fig. 10, by solving the equation $\mu(R_{\text{eff}, \theta}) = |G(y)| = 0.95$, we approximately obtain $y \approx 0.8257$. Therefore, we have $y = \sqrt{\frac{N^2 d^2 \cos^2 \theta}{2\lambda R_{\text{eff}}}} \approx 0.8257$. Moreover, since the array aperture is $D = Nd$, the effective Rayleigh distance is $R_{\text{eff}} \approx \frac{N^2 d^2 \cos^2 \theta}{2 \times 0.8257^2 \lambda} \approx \epsilon \cos^2 \theta \frac{2D^2}{\lambda}$, where $\epsilon = 0.367$. So the proof is completed.

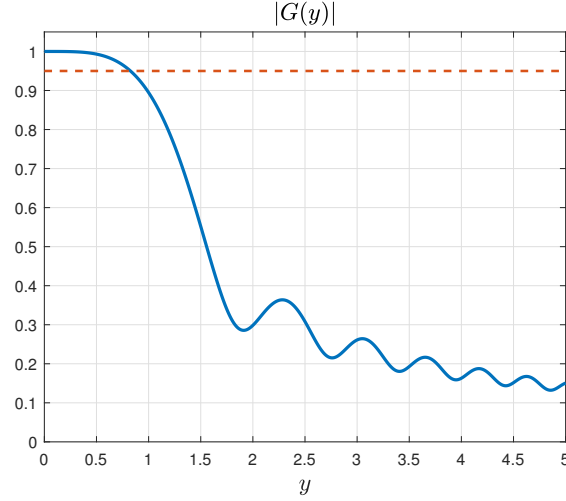


Fig. 10. The numerical results of $|G(y)|$

REFERENCES

- [1] R. W. Heath, N. González-Prelcic, S. Rangan, W. Roh, and A. M. Sayeed, “An overview of signal processing techniques for millimeter wave MIMO systems,” *IEEE J. Sel. Topics Signal Process.*, vol. 10, no. 3, pp. 436–453, Apr. 2016.
- [2] E. D. Carvalho, A. Ali, A. Amiri, M. Angelichinoski, and R. W. Heath, “Non-stationarities in extra-large-scale massive MIMO,” *IEEE Wireless Commun.*, vol. 27, no. 4, pp. 74–80, Aug. 2020.
- [3] “Radio stripes: re-thinking mobile networks,” 2019. [Online]. Available: <https://www.ericsson.com/en/blog/2019/2/radio-stripes>.
- [4] W. Tang, M. Z. Chen, X. Chen, J. Y. Dai, Y. Han, M. Di Renzo, Y. Zeng, S. Jin, Q. Cheng, and T. J. Cui, “Wireless communications with reconfigurable intelligent surface: Path loss modeling and experimental measurement,” *IEEE Trans. Wireless Commun.*, vol. 20, no. 1, pp. 421–439, Jan. 2021.
- [5] L. Zhang, M. Z. Chen, W. Tang, J. Y. Dai, L. Miao, X. Y. Zhou, S. Jin, Q. Cheng, and T. J. Cui, “A wireless communication scheme based on space- and frequency-division multiplexing using digital metasurfaces,” *Nat. Electron.*, vol. 4, p. 218–227, Mar. 2021.
- [6] S. Nie, J. M. Jornet, and I. F. Akyildiz, “Intelligent environments based on ultra-massive MIMO platforms for wireless communication in millimeter wave and terahertz bands,” in *Proc. IEEE International Conference on Acoustics, Speech and Signal Processing (IEEE ICASSP’19)*, May 2019, pp. 7849–7853.
- [7] A. R. Ndjiongue, T. M. N. Ngatched, O. A. Dobre, and H. Haas, “Towards the use of reconfigurable intelligent surfaces in VLC systems: Beam steering,” *arXiv preprint arXiv:2009.06822*, Sep. 2020.
- [8] V. Arun and H. Balakrishnan, “Rfocus: Beamforming using thousands of passive antennas,” in *Proc. 17th USENIX Symposium on Networked Systems Design and Implementation (NSDI’20)*, Feb. 2020, pp. 1047–1061.
- [9] A. Liao, Z. Gao, Y. Yang, H. H. Nguyen, H. Wang, and H. Yin, “Angle estimation for terahertz ultra-massive MIMO-based space-to-air communications,” *arXiv preprint arXiv:2108.00675*, Aug. 2021.
- [10] S. J. Maeng, Y. Yapıcı, İsmail Güvenç, A. Bhuyan, and H. Dai, “Precoder design for physical-layer security and authentication in massive MIMO UAV communications,” *arXiv preprint arXiv:2107.00799*, Jul. 2021.
- [11] S. Koenig, D. Lopez-Diaz, J. Antes, F. Boes, R. Henneberger, A. Leuther, A. Tessmann, R. Schmogrow, D. Hillerkuss,

- R. Palmer, T. Zwick, C. Koos, W. Freude, O. Ambacher, J. Leuthold, and I. Kallfass, "Wireless sub-THz communication system with high data rate," *Nat. Photonics*, vol. 7, p. 977–981, Oct. 2013.
- [12] H. Elayan, O. Amin, B. Shihada, R. M. Shubair, and M. Alouini, "Terahertz band: The last piece of RF spectrum puzzle for communication systems," *IEEE Open J. Commun. Society*, vol. 1, pp. 1–32, 2020.
- [13] T. S. Rappaport, Y. Xing, O. Kanhere, S. Ju, A. Madanayake, S. Mandal, A. Alkhateeb, and G. C. Trichopoulos, "Wireless communications and applications above 100 GHz: Opportunities and challenges for 6G and beyond," *IEEE Access*, vol. 7, pp. 78 729–78 757, 2019.
- [14] Z. Zhou, X. Gao, J. Fang, and Z. Chen, "Spherical wave channel and analysis for large linear array in LoS conditions," in *Proc. IEEE Globecom Workshops 2015*, Dec. 2015, pp. 1–6.
- [15] B. Friedlander, "Localization of signals in the near-field of an antenna array," *IEEE Trans. Signal Process.*, vol. 67, no. 15, pp. 3885–3893, Aug. 2019.
- [16] D. Tse and P. Viswanath, *Fundamentals of Wireless Communication*. Cambridge, U.K.: Cambridge Univ. Press, 2005.
- [17] K. T. Selvan and R. Janaswamy, "Fraunhofer and fresnel distances: Unified derivation for aperture antennas," *IEEE Antennas Propag. Mag.*, vol. 59, no. 4, pp. 12–15, Aug. 2017.
- [18] D. Headland, Y. Monnai, D. Abbott, C. Fumeaux, and W. Withayachumnankul, "Tutorial: Terahertz beamforming, from concepts to realizations," *APL Photonics*, vol. 3, p. 051101, May 2018.
- [19] F. Sohrabi and W. Yu, "Hybrid analog and digital beamforming for mmWave OFDM large-scale antenna arrays," *IEEE J. Sel. Areas Commun.*, vol. 35, no. 7, pp. 1432–1443, Jul. 2017.
- [20] L. Dai, J. Tan, and H. V. Poor, "Delay-phase precoding for wideband THz massive MIMO," *arXiv preprint arXiv:2102.05211*, Feb. 2021.
- [21] X. Gao, L. Dai, S. Zhou, A. M. Sayeed, and L. Hanzo, "Wideband beamspace channel estimation for millimeter-wave MIMO systems relying on lens antenna arrays," *IEEE Trans. Signal Process.*, vol. 67, no. 18, pp. 4809–4824, Jul. 2019.
- [22] G. Yasaman, S. Rabi, C. Aaron, K. Edward, and M. Daniel, "Single-shot link discovery for terahertz wireless networks," *Nat. Commun.*, vol. 11, no. 1, pp. 1–6, Apr. 2020.
- [23] Y. Chen, Y. Xiong, D. Chen, T. Jiang, S. X. Ng, and L. Hanzo, "Hybrid precoding for wideband millimeter wave MIMO systems in the face of beam squint," *IEEE Trans. Wireless Commun.*, vol. 20, no. 3, pp. 1847–1860, Mar. 2021.
- [24] X. Liu and D. Qiao, "Space-time block coding-based beamforming for beam squint compensation," *IEEE Wireless Commun. Lett.*, vol. 8, no. 1, pp. 241–244, Feb. 2019.
- [25] X. Yu, J. Shen, J. Zhang, and K. B. Letaief, "Alternating minimization algorithms for hybrid precoding in millimeter wave MIMO systems," *IEEE J. Sel. Topics Signal Process.*, vol. 10, no. 3, pp. 485–500, Mar. 2016.
- [26] H. Hashemi, T. Chu, and J. Roderick, "Integrated true-time-delay-based ultra-wideband array processing," *IEEE Commun. Mag.*, vol. 46, no. 9, pp. 162–172, Sep. 2008.
- [27] C. Lin, G. Y. Li, and L. Wang, "Subarray-based coordinated beamforming training for mmWave and sub-THz communications," *IEEE J. Sel. Areas Commun.*, vol. 35, no. 9, pp. 2115–2126, Sep. 2017.
- [28] J. Sherman, "Properties of focused apertures in the Fresnel region," *IRE Trans. Antennas Propag.*, vol. 10, no. 4, pp. 399–408, Jul. 1962.
- [29] D. Fattal, J. Li, Z. Peng, M. Fiorentino, and R. G. Beausoleil, "Flat dielectric grating reflectors with focusing abilities," *Nat. Photonics*, vol. 4, p. 466–470, May 2010.
- [30] J. Tan and L. Dai, "Wideband beam tracking in THz massive MIMO systems," *IEEE J. Sel. Areas Commun.*, vol. 39, no. 6, pp. 1693–1710, Jun. 2021.
- [31] R. J. Mailloux, *Phased Array Antenna Handbook*. Norwood, MA, USA: Artech House, 2005.
- [32] S. Mumtaz, J. Rodriguez, and L. Dai, *MmWave Massive MIMO: A Paradigm for 5G*. Academic Press, Elsevier, 2016.

- [33] Z. Zhang, L. Dai, X. Chen, C. Liu, F. Yang, R. Schober, and H. V. Poor, “Active RIS vs. passive RIS: Which will prevail in 6G?” *arXiv preprint arXiv:2103.15154*, Mar. 2020.
- [34] M. Cui and L. Dai, “Channel estimation for extremely large-scale MIMO: Far-Field or Near-Field?” *arXiv preprint arXiv:2108.07581*, Aug. 2021.